Backstop geometry and accretionary mechanics of the Sunda margin

Heidrun Kopp

GEOMAR Research Center for Marine Geosciences, Kiel, Germany

Nina Kukowski

GFZ GeoForschungsZentrum, Potsdam, Germany

Received 29 May 2002; revised 14 March 2003; accepted 18 July 2003; published 11 December 2003.

[1] The convergent Sunda margin off Indonesia displays all geological features characteristic of an accretion-dominated subduction zone. A combined interpretation of prestack depth-migrated seismic reflection data and velocity information gained from refraction studies is supplemented by high-resolution bathymetric data and for the first time allows the exact mapping of backstop regimes. Initially, the outer high evolved as material was pushed against a static rigid arc framework backstop underlying a forearc basin. Increasing material strength of the outer high due to lithification formed a dynamic backstop, which controls accretion today. An out-of-sequence thrust marks the transition from the recent active frontal accretionary prism to the outer high and may be traced in the seismic and bathymetric data over the whole extent of the study area. The existence of a static as well as a dynamic backstop controls the forearc geometry and is associated with the segmentation of the forearc, which is observed in regimes of frontal as well as of oblique subduction. Mass balance calculations, which account for porosity changes and metamorphism, indicate a subduction history dominated by accretionary processes since the late Eocene. Accretion is associated with the low values of basal friction inferred for the Sunda margin. Structural investigations of conjugate fault planes indicate a very weak basal detachment. Effective stress analyses reveal that intrinsically weak material causes the high strength ratio of the detachment to the overlying sediments, whereas overpressuring within the frontal accretionary prism is negligible. *INDEX TERMS:* 8020 Structural Geology: Mechanics; 8045 Structural Geology: Role of fluids; 8010 Structural Geology: Fractures and faults; 8015 Structural Geology: Local crustal structure; 9340 Information Related to Geographic Region: Indian Ocean; *KEYWORDS:* morphotectonics, mass balance, effective stress analysis, backstop geometry, prestack depth migration, wide-angle seismics. **Citation:** Kopp, H., and N. Kukowski, Backstop geometry and accretionary mechanics of the Sunda margin, *Tectonics*, *22*(6), 1072, doi:10.1029/2002TC001420, 2003.

0278-7407/03/2002TC001420

1. Introduction

[2] A wide variety of tectonic styles at subduction zones, including erosional and accretionary regimes, has been documented by seismic data. Most subduction zone histories are nonuniform and are characterized by alternate phases of subduction erosion and subduction accretion. The fundamental role of a mechanical boundary or ''backstop'' on the evolution of forearc geometries, especially on the evolution of a structural outer high as is characteristic for many accretionary type margins, has been recognized by *Dahlen* [1990]. The term backstop defines a region within a forearc that is characterized by an increased yield strength compared to the region trenchward of it and thus its ability to support larger deviatoric stresses. The seaward material then deforms at a greater rate and thus presents a contrast in strain rate to the landward section [*Davis*, 1996], resulting in a segmentation of an accretionary complex, as described for the Sunda margin by *Schlüter et al.* [2002]. Zones of distinct strength contrast may result from changes in lithology and thus naturally coincide with contrasts in material properties such as density and seismic velocity. A variety of materials may act as backstop, ranging from arc framework (continental or oceanic) to features like an allochthonous terrane or well-lithified paleoaccreted material displaying a higher degree of consolidation and densification than the more recently accreted sediment seaward of it. The kinematic discontinuities which form a backstop may be ''static'', as would be the case for continental arc basement, or ''dynamic'' and thus still deforming, though at a slow rate, as may be expected for compacted accreted material resulting from an earlier phase of accretion. Though numerous backstop geometries have been modeled for different subduction settings, their identification in nature, especially for deeper lying backstops, is often difficult due to the limited penetration of seismic reflection data. Shallow backstops at less than 10 km depth have successfully been imaged, e.g., off Peru [*von Huene et al.*, 1988], off Alaska [*Fruehn et al.*, 1999], and in the Ryukyu forearc [*Font et al.*, 2001]. In this study, the existence of multiple kinematic boundaries in a single subduction complex is inferred from the combined interpretation of seismic reflection profiles and deeply

penetrating seismic refraction data as well as high-resolution bathymetry from the Sunda margin off Indonesia. The seaward dipping arc basement acts as a strong static backstop, whereas a weaker and younger backstop composes the fossil part of the accretionary wedge. It will be shown in this paper that the existence of the main forearc structures (i.e., forearc basin and outer high) is fundamentally linked to the presence of the static arc framework backstop. The younger minor backstop is a dynamic, still deforming zone of low strain rate along a kinematic boundary in the segmented forearc. The presence of a strong static backstop as well as a weaker dynamic backstop plays the crucial role in the development of tectonic features along this margin, whereas the oblique component of subduction results in transpressional expressions of the plate collision.

[3] An additional aspect of this study investigates the influence of the varying mechanical properties on the segmentation of the forearc and the corresponding morphological attributes. Implications on accretionary mechanics are drawn from structural relations of conjugate failure planes. Conjugate forethrusts and back thrusts are imaged in a depth section near the Sunda deformation front and are employed in an effective stress analysis.

2. Tectonic Setting of the Sunda Convergent Margin

[4] The Sunda Arc convergent margin curves along the islands of Sumatra and Java in Indonesia and marks the collision zone between the Indo-Australian plate and Eurasia. This sector of the subduction system has been active since middle Tertiary time, as inferred from dating of the Sunda system volcanism [*Hamilton*, 1988]. The northern and central part of the margin, from northern Sumatra to western Java, has been the site of geophysical and geological research, mainly attracted by the unique setting of an increasing subduction obliqueness to the north [*Fitch*, 1972; *Hamilton*, 1979; *Huchon and Le Pichon*, 1984; *McCaffrey*, 1992; *Diament et al.*, 1992; *Malod and Kemal*, 1996]. While the nature of the outer high, which is present all along the subduction zone and emerges subaerially as a chain of islands off Sumatra, has long been debated, recent studies support an accretionary origin of the outer high and a subduction history dominated by accretion over erosion. At present times, the central Sunda margin may be described as accretionary and thus, in view of the large fraction of modern subduction zones that have been found to be erosional [*von Huene and Scholl*, 1991; *Ranero and von Huene*, 2000], represents one end-member of convergent margins. It displays a deep trench, an actively accreting frontal prism and a massive fossil outer high adjacent to a well-developed forearc basin, which carries several kilometers of sediment fill [*Moore et al.*, 1980]. Numerous geological parameters change along the arc, including the age of the oceanic plate and the convergence rate, both of which increase toward Java and Bali, while the thickness of the incoming ocean basin deposits and trench fill decrease in the same direction [*Hamilton*, 1979]. The curvature of the trench results in regimes of frontal subduction off Java to oblique subduction off Sumatra [*Fitch*, 1972; *Moore et al.*, 1980; *McCaffrey*, 1996; *McCaffrey et al.*, 2000]. The central part of the Sunda margin marks the onset of oblique subduction south of the Sunda Strait [*Malod et al.*, 1995]. Though the oblique collision results in the development of the lithospheric-scale Sumatra Fault [*Sieh and Natawidjaja*, 2000] and possibly the offshore Mentawai Fault zone [*Diament et al.*, 1992], structural effects from the change in orientation of the trench on the adjacent subduction complex are limited and not yet clearly evidenced. The existence of the highly deformed outer high and the seemingly paradoxical presence of mainly undeformed sedimentary units in the adjacent forearc basin result from the influence of a static backstop as shown here which is formed by the arc framework of the upper plate's leading edge. Refraction seismic studies have shown that the arc basement is continental in nature along southern Sumatra, changing to an oceanic character off western Java [*Kopp et al.*, 2001, 2002]. The outer high, which represents the fossil part of the accretionary wedge, is of Eocene-Oligocene age [*Pubellier et al.*, 1992; *Samuel and Harbury*, 1996] and most likely composed of accreted material, as suggested by field mapping [*Moore and Karig*, 1980], refraction and gravity data [*Kieckhefer et al.*, 1981; *Kopp et al.*, 2001, 2002], though deep drilling information is not available. Seismic investigations in the forearc basin off northern Sumatra have been correlated to drilling information and suggest an Oligocene age for the oldest sediments trapped here [*Beaudry and Moore*, 1981, 1985; *Izart et al.*, 1994; *Schlüter et al.*, 2002]. An Oligocene origin has also been attributed to the oldest sediments in the Sunda Strait [*Diament et al.*, 1990; *Lelgemann et al.*, 2000].

3. Data

3.1. Bathymetry

[5] A grid of bathymetric data, mostly along single ship tracks, was acquired along the central portion of the Sunda margin (Figure 1) in late 1998 and early 1999. Full coverage was gained in an area off southern Sumatra between 102°E to 103°E and 6°25′S to 7°10′S as well as off western Java at about 9.3°S. The swath mapping was achieved using R/V Sonne's onboard Hydrosweep multibeam system [*Grant and Schreiber*, 1990] with a 90° beam angle. Subsequent processing of each sweep was conducted using mbsystem [*Caress and Chayes*, 1996] and GMT [*Wessel and Smith*, 1991]. Sonic velocity was measured employing a CTD instrument. To guarantee preservation of morphological detail, no data smoothing or filtering was performed. Track noise of overlapping parts of adjacent tracks in perspective views (Figures 2 and 3) then allows an optical assessment of peak noise level.

3.2. Seismic Data and Processing

[6] Seismic wide-angle data were acquired along the black tracks shown in Figure 1 using a total of 40 ocean bottom hydrophone and seismometer stations [*Flueh and Bialas*, 1996; *Flueh and Shipboard Science Party*, 1999]. Seismic reflection data were collected on coincident lines

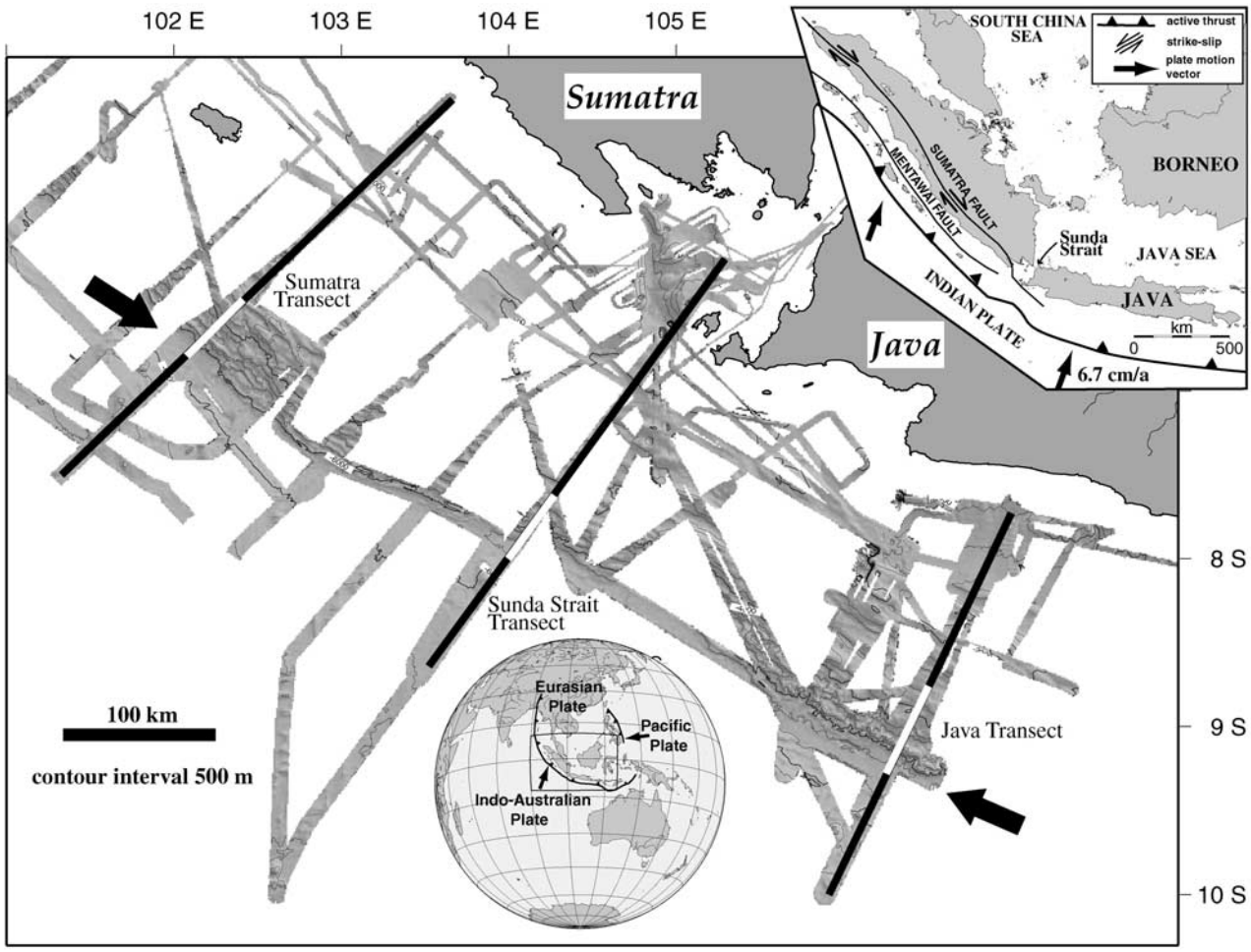

Figure 1. Bathymetric survey conducted along the central Sunda margin. Thick black lines depict the location of the seismic refraction profiles, and white sections along these lines represent the extent of the depth-migrated multichannel data. The Sunda Strait Transect is presented in Figure 4, and the Sumatra and Java Transects are shown in Figure 5. Arrows indicate the view direction for the 3-D bathymetric images presented in Figures 2 and 3.

by the BGR, Hannover, Germany [*Reichert et al.*, 1999].The entire data set and processing are described in detail by *Kopp et al.* [2001, 2002]. For this study, the white portions along the seismic tracks in Figure 1 were prestack depth migrated. The migrated reflection data are shown in Figures 4 and 5. An iterative migration procedure was applied which uses seismic velocities constrained by focusing analyses and common reflection point gathers [*Mackay and Abma*, 1993] as well as velocity information gained from the wide-angle data. Seismic velocities used during the migration process are interval velocities. The energy of a reflection point in the subsurface is focused using a range of velocities until an optimal image is achieved, which provides the highest energy at zero offset. Using an ideal velocity, the reflection position will be corrected. This in turn will yield better constraints on velocities during the next iteration and ray paths are determined more accurately. Prestack depth migration thus images complex dipping structures even in the presence of a strong lateral velocity gradient far better than conventional poststack migration procedures.

3.3. Seismic Sections: Tectonic Interpretation

[7] The seismic sections derived from prestack depth migration offer the precise image of the active frontal accretionary prism allowing the recognition of several common tectonic features characteristic for this margin. Three adjacent segments are recognized on all seismic sections (Figures 4 and 5) and will be described based on the interpretive section of the Sunda Strait profile presented in Figure 4. Segment I includes the sediment flooded trench. Vague seaward and landward vergent faults, originating several tens to hundreds of meters below the seafloor, cut the trench sediment sequences down to near the top of the igneous crust and mark the onset of deformation in the protothrust zone. The devel-

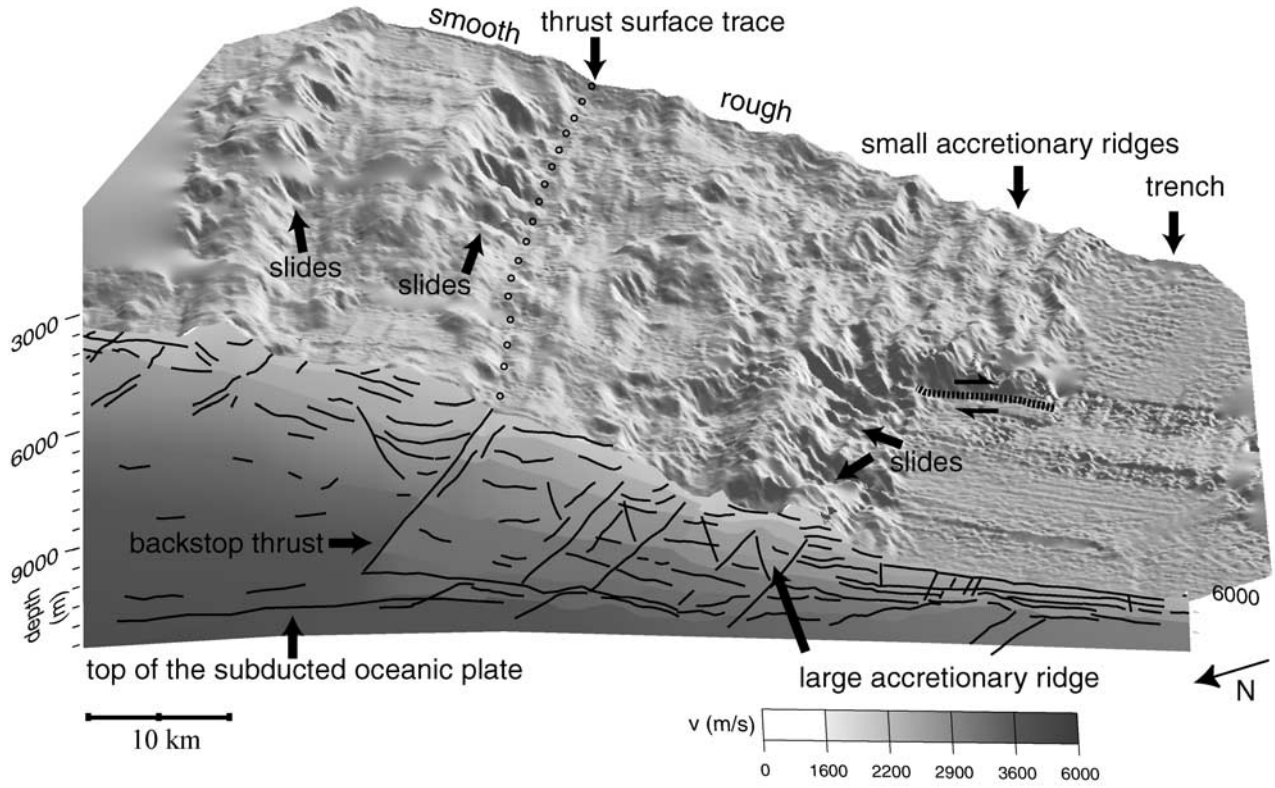

Figure 2. Three-dimensional bathymetric image of the deformation front and frontal accretionary prism off southern Sumatra viewed from the northwest. A line drawing of the depth-migrated profile and the corresponding velocity field are displayed in the cross section in the foreground. An increase in seismic velocities across an out-of-sequence thrust indicates a positive arcward gradient in material strength. The corresponding surface expression of this backstop thrust may be traced along the whole extent of the bathymetry survey as indicated by the circles. The striking retreat of the deformation front of about 8 km marks a transfer fault connecting supercritical portions of the slope characterized by slumps and slides in the NW to regularly spaced accretionary ridges in the SE.

opment of a pair of conjugate forethrust and back thrust manifests the inception of faulting at the deformation front. The occurrence of steep sets of conjugate reverse faults represents an extremely unusual geometry for a frontal zone of shallow thrusts above a décollement. The Sunda Strait line shows the finest example of a conjugate thrust pair near the deformation front (Figure 4). As addition of new material progresses, the shallower dipping forethrust becomes the dominant fault. Segment II forms the active accretionary domain and is characterized by tilted, regularly spaced thrust slices. These are separated by thrust faults (at times accompanied by secondary branch thrusts), which may cause minor offsets of the seafloor and cut the complete accreted wedge down to a detachment surface. These high-amplitude reflections are characteristic for a classical imbricate accretionary prism [*Davis and Hyndman*, 1989; *Moore et al.*, 1990; *von Huene and Klaeschen*, 1999] and indicate shear zones, which actively retain a constant surface slope along this segment. The increasing thrust length indicates the laterally increasing material strength due to dewatering which is highly effective along faults acting as conduits [*von Huene and Klaeschen*, 1999].

[8] Along all lines, an out-of-sequence thrust separates segments II and III, which correspond to the active accretionary domain and the fossil outer high, respectively (Figures 4 and 5). The difference in surface slope from segment II to segment III as well as out-of-sequence thrusting implies arcward variations in material properties [*Gutscher*, 1996]. A shallowing of the surface slope in segment III marks a gradual transition to material of greater strength, for which the taper must be adjusted. Little coherent imaging is resolved in the different structural style of segment III. Formerly generated, additional out-of-sequence thrusts are present in segment III, these are rotated and most of the time nonactive, as the outer high forms the fossil part of the accretionary prism [*Schlüter et al.*, 2002]. The possible intermittent reactivation of these faults helps adjust the taper [*Lohrmann et al.*, 2002], thus deformation results in vertical uplifting of the outer high rather than horizontal shortening, which is predominant in segment II of the frontal active accretionary domain. Overall, active

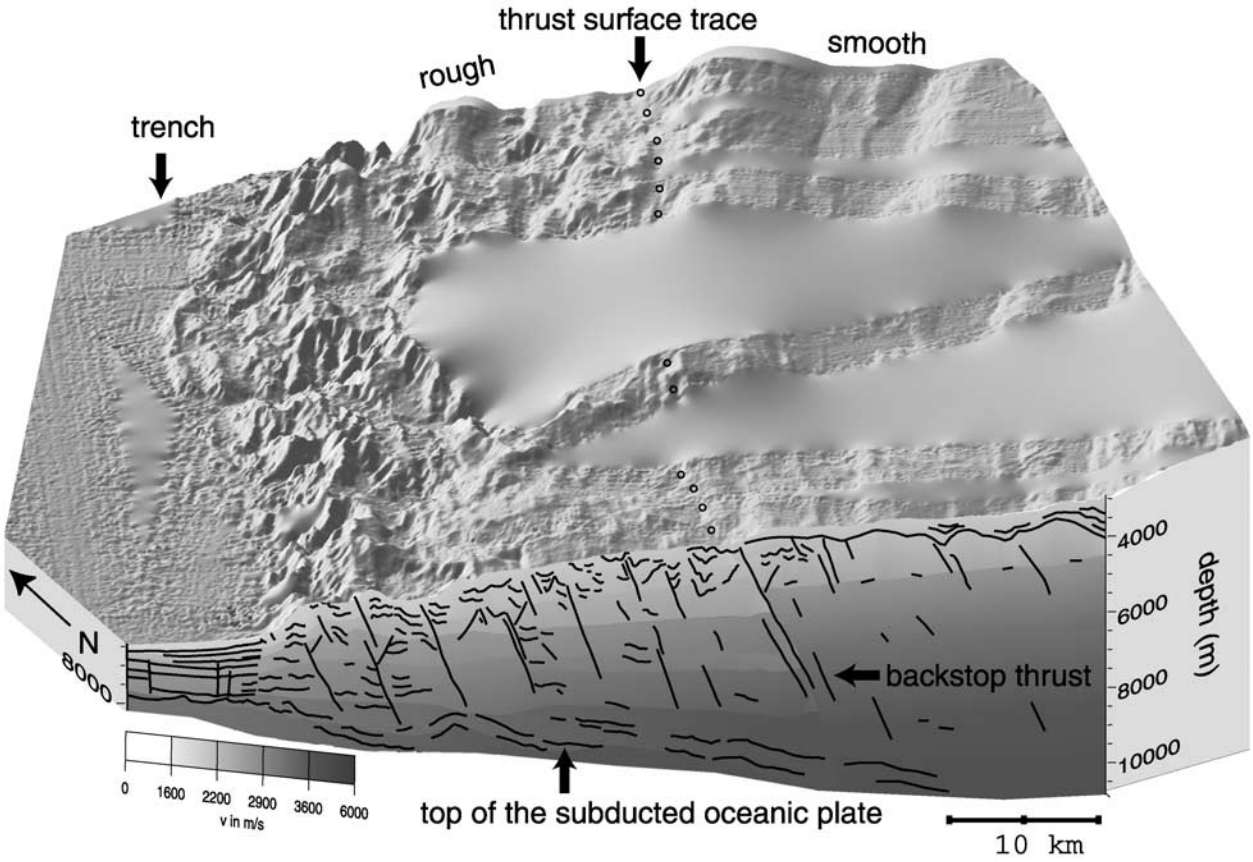

Figure 3. Bathymetric view of the deformation front and lower slope off Java viewed from the southeast. Please refer to Figure 2 for display information. An out-of-sequence thrust marking the seaward limit of the dynamic backstop corresponds to an increase in seismic velocities and is also recognized in the surface morphology. The rough topography in between the trench and the surface trace of the out-of-sequence thrust changes to a smooth seafloor arcward of the backstop thrust, where the intense fault activity is reduced.

faulting along the outer high is much reduced compared to segment II as the carbonate sedimentary cover [*Reichert et al.*, 1999] of the outer high is commonly not affected by the identified thrusts which cut the solidified portion of the outer high. Seismic velocities derived from prestack depth migration indicate a significant lateral velocity increase over the transition from segment II to segment III (Figures 2 and 3), which manifests the elevated material strength of the highly compacted accreted mass that comprises the outer high. Thus segment III acts as a transient backstop to the newly accreted material of segment II, as discussed further below.

[9] A detachment surface is most coherently imaged along the Sunda Strait segment, however, along all three profiles approximately 11–14% of the input sediment sequence is underthrust in a subduction window defined through the distance to the detachment surface and the top of the igneous crust beneath segment II and segment III (Figures 4 and 5). This low percentage of subducted material is to be expected for margins with large accretionary prisms, as observed along the Sunda margin [*von Huene and Scholl*, 1991]. Possible underplating of this material underneath the outer high is not resolved in our data.

4. Static and Dynamic Backstops: Control on Forearc Geometry

[10] The extensive folding and faulting of the incoming trench sediments in the vicinity of the deformation front is documented in the highly variable morphology here (Figures 2 and 3), which smoothes further landward in segment III, where active faulting of the accreted strata is reduced or ceases (Figures 4 and 5). Recent accretionary ridges are only recognized along the southeastern portion of the Sumatran transect (Figure 2). Velocities increase with depth, as may be expected from the larger overburden, but show little lateral variation up to the location of the out-of-sequence thrust. The thrust surface trace is clearly visible in the seafloor topography and may be followed along the whole extent of the bathymetry survey (black circles in Figures 2 and 3). It marks the seaward limit of the dynamic

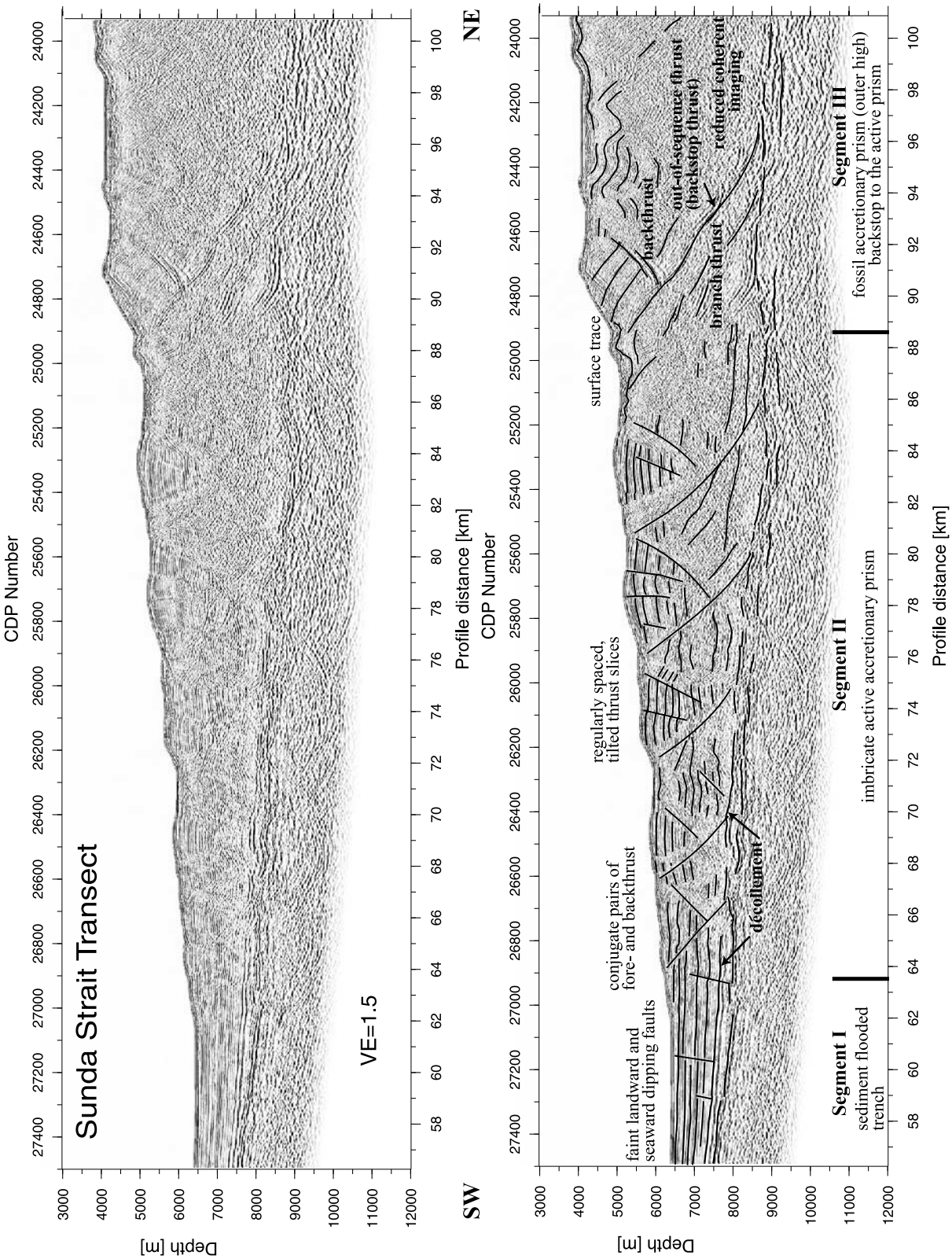
Sunda Strait Transect
VE=1.5
CDP Number
Profile distance [km]
Depth [m]
SW
NE
surface trace
backthrust
out-of-sequence thrust (backstop thrust)
branch thrust
reduced coherent imaging
regularly spaced, tilted thrust slices
conjugate pairs of fore- and backthrust
faint landward and seaward dipping faults
décollement
Segment I
sediment flooded trench
Segment II
imbricate active accretionary prism
Segment III
fossil accretionary prism (outer high) backstop to the active prism

backstop (segment III) (Figures 4 and 5). The sharp lateral velocity contrast across the out-of-sequence thrust is also recognized in the wide-angle sections covering these lines (Figure 6). The dynamic backstop is composed of fossil accreted material, which shows a positive landward gradient in the rate of lithification. Any nonuniform phase of accretion will cause a discontinuity in lithification and thus a contrast in strength sufficient to classify the landward portion as backstop to the unconsolidated ocean basin deposits and turbidites accreted at the deformation front. Deformation of the dynamic backstop is still occurring through intermittent reactivation of older thrusts in segment III. However, the rate of deformation is much lower than within the frontal accretionary prism. The frontal prism will have stress conditions consistent with predominantly arcward thrust dips [*Byrne et al.*, 1993], as established by the seismic images shown in Figures 4 and 5. This preferred dip will generally not extend past the dynamic backstop and is manifested in the area of intense faulting across the active accretionary domain of segment II. The outer high, which is the fossil portion of the accretionary wedge (i.e., the dynamic backstop), then experiences less arcward dipping faulting, as is also evident from the morphology in places where the seafloor roughness of the sediments overlying the dynamic backstop landward of the out-of-sequence thrust is reduced compared to the seaward portion (Figures 2 and 3).

[11] The downward limit of the dynamic backstop is provided by the subducting oceanic plate; the landward termination is marked by the leading edge of the upper plate arc framework underlying the forearc basin (Figure 6). This boundary between the outer high, which composes the dynamic backstop, and the arc framework, which acts as a static backstop, corresponds to a second kinematic boundary within this margin. The change in composition of this static backstop from continental arc framework off Sumatra to oceanic arc basement off western Java, as induced from refraction and gravity data [*Kopp et al.*, 2001, 2002] is subordinate for the development of the subduction zone complex, as a backstop is not linked to a specific composition but is characterized by a strength contrast, given here between the lithified paleoaccreted mass of the outer high and the stronger arc framework. The initial development of the outer high results from the gradual increase in both strength and bulk density as the material is compacted with depth and distance from the deformation front [*Byrne et al.*, 1993]. When this gradual increase in rock strength is replaced by a sharp transition at the static backstop, which can support larger loads, the increased net horizontal load is accommodated without further buildup of topography. As a result, the outer high develops above the seaward end of the static backstop. The backstop geometry found along the central Sunda margin (Figure 6) puts the toe of the static backstop near the top of the subducted oceanic plate (at profile km 130 for the Sumatra and Sunda Strait transects and at 105 km for the Java transect, compare Figure 6), so that little sediment is thrust beneath the backstop (trenchward dipping type I geometry of *Byrne et al.* [1993]). The static backstop casts a stress shadow over the area above itself, allowing the presence of a forearc basin which will experience no or little deformation as sediments are deposited within it [*Malavieille*, 1984; *Byrne et al.*, 1993]. The backstop then supports most of the regional horizontal compressive plate boundary stresses. The models presented in Figure 6 show an almost perfect alignment of the crest of the outer high to the toe of the static backstop, as has been predicted from numerical and sandbox modeling [*Byrne et al.*, 1993]. As the outer high is uplifted, the seaward part of the forearc basin experiences some uplift and deformation, resulting in landward tilting and pinching out of the older strata near the outer high as seen on line SO137-03 in *Kopp et al.* [2002].

5. Quantitative Estimates From Volume Balance Calculations

[12] Geological sampling on Nias Island, which forms part of the Outer High off northern Sumatra, suggest an Eocene-Oligocene age for this fossil part of the accretionary prism, i.e., recent dynamic backstop [*Moore and Karig*, 1980; *Moore et al.*, 1982; *Pubellier et al.*, 1992; *Samuel and Harbury*, 1996], which corresponds to a proposed Eocene onset or reinitiation of the current subduction phase [*Hamilton*, 1988; *Schlüter et al.*, 2002]. The forearc basin infill is younger as an Oligocene origin for the oldest sediment has been inferred [*Beaudry and Moore*, 1981, 1985; *Diament et al.*, 1990; *Lelgemann et al.*, 2000].

[13] The exact mapping of the tectonic regime along the central Sunda margin allows observations on the period of accretion on this convergence zone. The pure dimensions of the fossil accretionary wedge or outer high with a thickness of more than 15 km (compare Figure 6) suggest a long period of convergent processes dominated by accretion, which would be necessary to accumulate the amount of material observed here today. Mass balance calculations will give a rough estimate on the percentage of sediment subducted beneath the backstop and material accreted to form today's accretionary complex. Little information is available on the variation of geological parameters with time, foremost the convergence rate and the amount of

Figure 4. (opposite) Prestack depth-migrated section of the multichannel profile off the Sunda Strait. An arcward increase in material strength results in a segmentation of the margin. Faint seaward and landward dipping faults cut the trench fill in the protothrust zone of segment I, indicating the first stages of faulting. The deformation front marks the onset of faulting in conjugate pairs of forethrusts and back thrusts. The frontal active accretionary prism (segment II) is composed of tilted thrust slices separated by regularly spaced thrust faults. The transition to the fossil accretionary prism of the outer high is marked by a prominent out-of-sequence thrust. Segment III forms the backstop to the frontally accreted material and displays much reduced tectonic activity mainly manifested in the occasional reactivation of previous thrusts which helps adjust the taper.

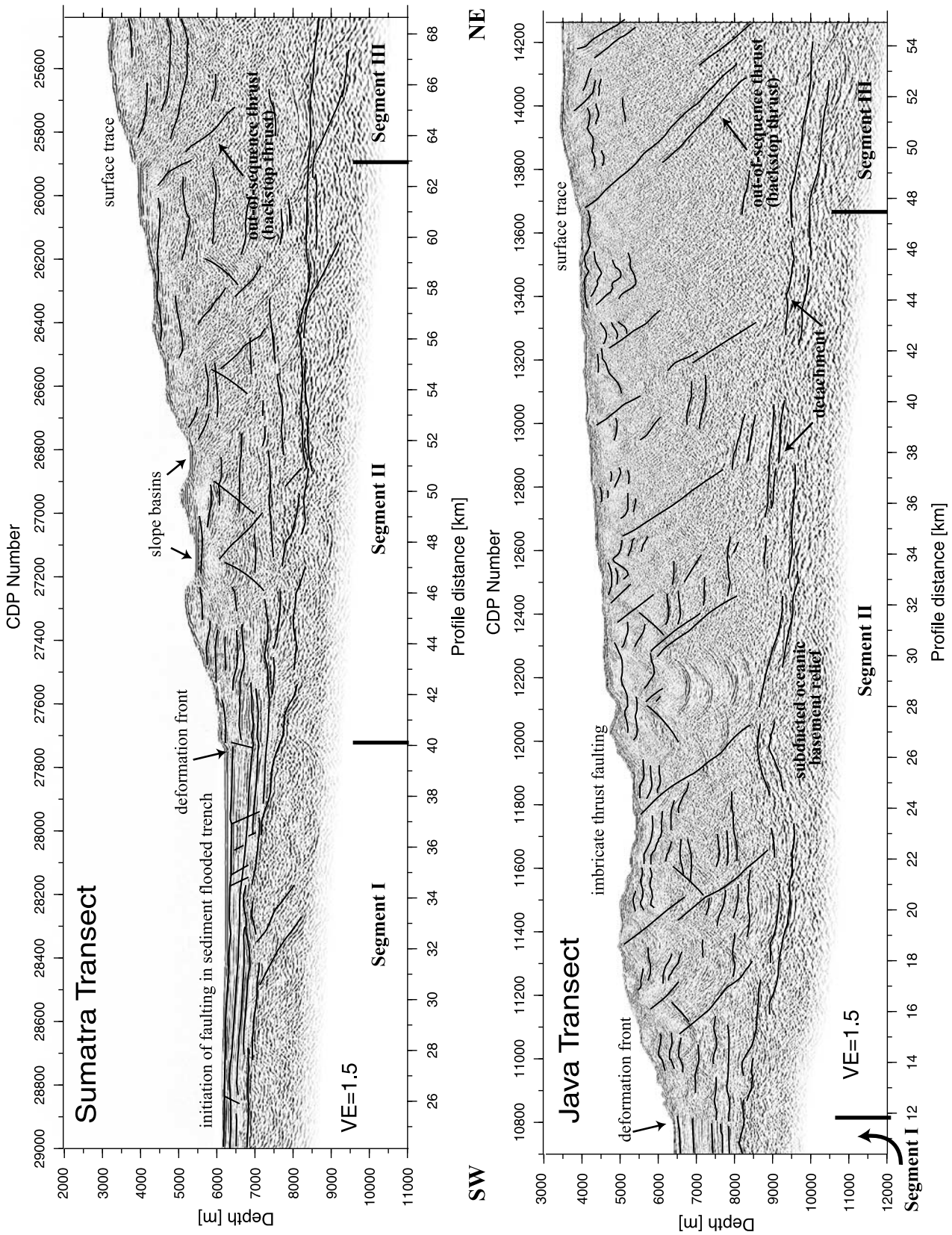
Sumatra Transect
CDP Number
Depth [m]
Profile distance [km]
surface trace
slope basins
deformation front
initiation of faulting in sediment flooded trench
out-of-sequence thrust (backstop thrust)
Segment I
Segment II
Segment III
VE=1.5
SW
NE
Java Transect
CDP Number
Depth [m]
Profile distance [km]
surface trace
imbricate thrust faulting
deformation front
out-of-sequence thrust (backstop thrust)
subducted oceanic basement relief
detachment
Segment I
Segment II
Segment III
VE=1.5

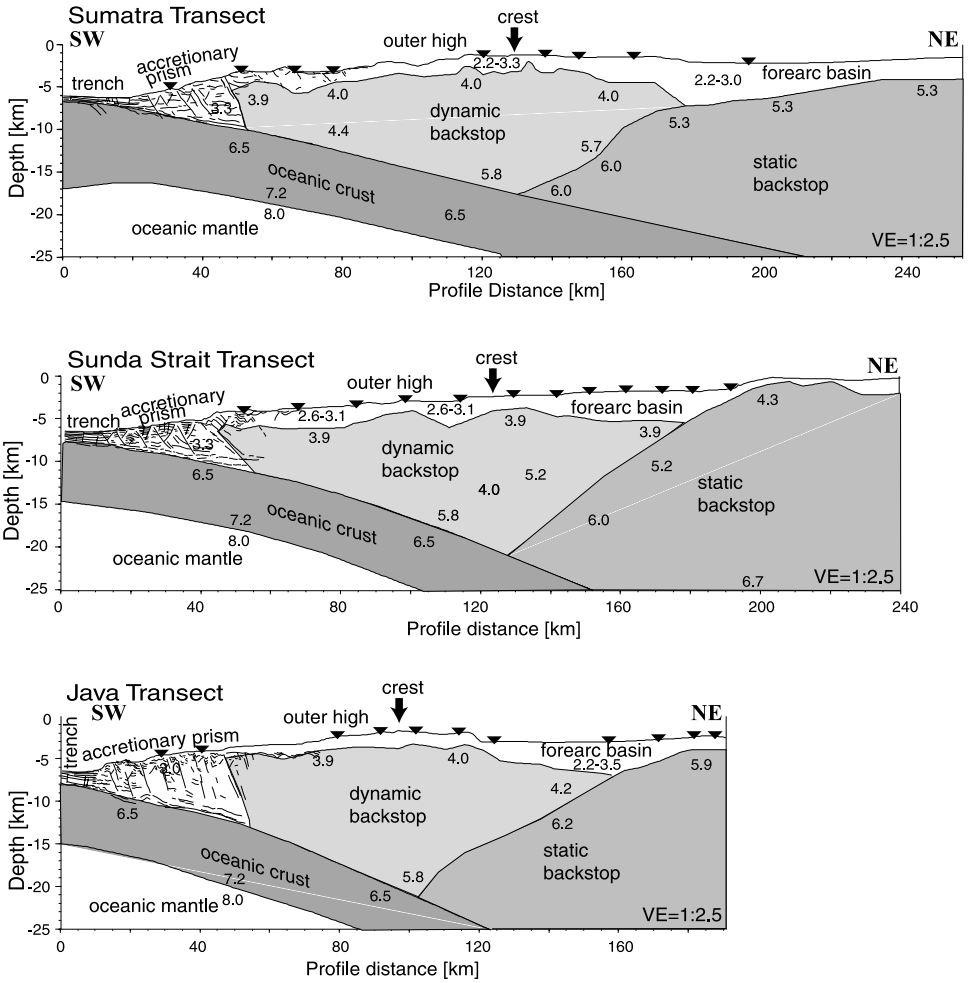

Figure 6. Structural models for the Sumatra, Sunda Strait, and Java sector, respectively. The line drawing of the depth-migrated multichannel data is incorporated near the seaward portion of the subduction zone. The extent of the dynamic and static backstops has been inferred from refraction seismic data and gravity modeling. Velocity labels are given in km s^{-1}. Inverted triangles depict OBH positions. The consecutive shallowing of the surface slope from the deformation front to the forearc basin is a response to changing material properties within the wedge and along the base. The coarse structural features observed along the margin include the active frontal accretionary prism, the fossil outer high, which is of accretionary origin, and the deep forearc basin. The development of the morphological outer high results from the presence of the static backstop of arc framework, which sheds a stress shadow to the overlying area, where a forearc basin carrying undeformed sedimentary strata develops. The dynamic backstop evolves from the well-lithified fossil accretionary wedge.

sediment input into the trench. Today's conditions are well known from numerous geophysical and geological studies and are thus applied to the volume estimations. However, severe limitations on any mass balance calculations result from the long period considered, as any tectonic framework will not have remained uniform. Today, the convergence rate increases from 6.3 cm/yr off southern Sumatra to 6.7 cm/yr off western Java [*Prawirodirdjo et al.*, 2000; *Tregoning et al.*, 1994]. The trench fill along the central Sunda margin decreases toward the east, as the sediment

Figure 5. (opposite) Prestack depth-migrated sections of the MCS profiles off southern Sumatra (upper image) and off Java (lower image). Similar structural features as along the Sunda Strait line are recognized. The frontal active accretionary prism (segment II) is separated from the stronger material of the backstop (segment III) by an out-of-sequence thrust. The increased material strength may support a narrower wedge along segment III, resulting in a decreased surface slope. Imbrication of segment II along regularly spaced thrust faults affects the whole accreted section down to the décollement, indicating near constant material properties for the entire wedge.

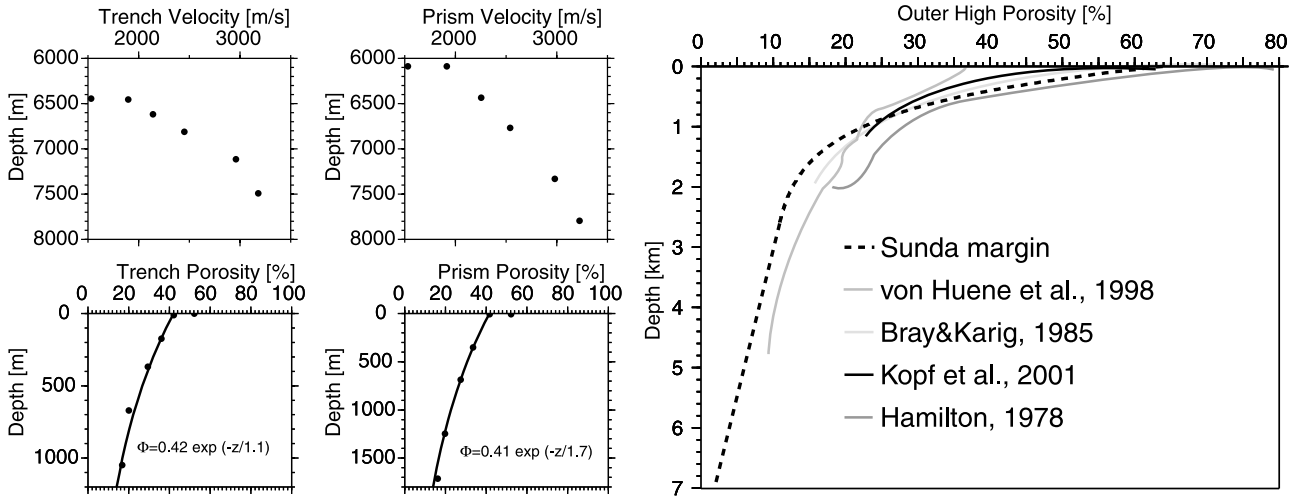

Figure 7. Porosity-depth relations for segments I to III of the margin. In the trench and lower accretionary prism, porosities are inferred from seismic interval velocities gained during prestack depth migration, which are transformed into porosities using a standard velocity-density relationship. Porosities Φ follow an exponential decay curve according to Athy's law. Along the outer high, exponential porosity decay in the upper 2.5 km is assumed, followed by a linear decay to 7 km depth (dashed curve). Below 7 km, porosities are negligible. Porosity-depth relations from other margins are displayed for comparison.

input from the Ganges-Bahmaputra system is reduced. A decreasing average trench fill from 1.3 km off Sumatra to 1.1 km off Java is used for the following discussion. These average values must be assumed, as the trench fill observed along the seismic lines shown here represent only a "snapshot" in time. Earlier investigations have shown that the ocean basin deposits input into the trench show a highly variable thickness on the oceanic plate seaward of the trench, ranging from 0 m to 900 m [*Kopp et al.*, 2001], thus the momentary trench fill does not reflect the overall decreasing sediment availability to the east. An areal balancing of the outer high (i.e., the dynamic backstop) is based on the combined reflection-refraction models presented in Figure 6 for which the estimated area was calculated from the pixel information contained in the graphical display of the model. This area estimated from the 2D display is then normalized to trench units to yield mass volume per trench kilometer. The observed volume of the outer high must be balanced against the trench input to derive the approximate period of accretion necessary to accumulate the observed accreted mass volume. To account for the varying pore space due to dehydration in the trench sediment and the outer high, the observed volumes are corrected to 0% porosity volume and thus converted to a solid mass equivalent for which the values derived for the trench and the outer high may be balanced directly. Today's volumes are derived from the pixel information contained in Figure 6, where a 10 × 10 km reference box contains 2352 pixels. As is obvious from Figure 6, the volume of the outer high decreases to the southeast, which corresponds to the pixel-derived mass volume values of 1372 km^3 per trench kilometer off southern Sumatra, 1210 km^3 off Sunda Strait and 967 km^3 off western Java. This also corresponds to the decreasing lateral extent of the dynamic backstop from 130 km off Sumatra to 94 km off Sunda Strait and 67 km off western Java. Reduction of the observed volumes to their solid mass equivalents is based on an empirical porosity-depth relationship (Figure 7) that was defined based on general information on sediment porosity in accretionary wedges and on laboratory measurements of porosity from Nias Island samples [*Bray and Karig*, 1985]. The porosity-depth curve is divided into four depth domains (a–d) for which different decay functions apply (Table 1): exponential porosity loss resulting from lithification is expected in a depth range down to 2.5 km below the surface (domain a); from 2.5 to 7 km depth (domain b), a linear decrease is assumed (Figure 7). At greater depth between 7 and 14 km (domain c), pore space is neglectable. Below 14 km depth (domain d), an increase in volume averaging approximately

Table 1. Porosity Decay Functions[a]

	Exponential Decay Function	Linear Decay Function	Assumed Constant Porosity
Outer high			
Domain a, 0–2.5 km	$\Phi = 0.6 \exp(-1.437z - 0.1) + 0.16$		
Domain b, 2.5–7 km		$\Phi = (z - 8)/50$	
Domain c, 7–14 km			$\Phi = 2\%$
Domain d, >14 km[b]			
Trench	$\Phi = 0.42 \exp(-z/1.1)$		
Frontal prism	$\Phi = 0.41 \exp(-z/1.7)$		

[a]Here Φ is porosity, and z is depth.
[b]Metamorphic processes leading to an assumed 1% volume increase.

Table 2. Mass Volumes

Area	Observed Volume, km^3	Solid Mass Equivalent, km^3
Sumatra	1372	1207
Sunda Strait	1210	1083
Java	967	871

1% resulting from metamorphic processes is included in the volume balancing. A solid mass volume for the dynamic backstop or outer high then is derived from the observed volume (corresponding to the four depth domains) and converted to a solid mass equivalent (Table 2) of 0% porosity by applying the porosity decay relationships applicable to the different depth domains.

[14] The derived solid mass volume comprises the fossil accretionary ridge which today forms the dynamic backstop and must thus be balanced against the input sequence (1.3 km off Sumatra, 1.25 km off Sunda Strait, 1.1 km off Java), which is converted to its solid mass equivalent using an exponential porosity-depth decay based on Athy's law (Figure 7, trench porosity) [*von Huene et al.*, 1998]. Seismic velocities derived from the focusing analyses performed during prestack depth migration were converted to porosities based on a standard velocity-density relationship [*Hamilton*, 1978; *Fruehn et al.*, 1997] using a pore water density of 1050 kg m^{-3} and an average grain density of 2760 kg m^{-3} for sediment. Global glacial conditions resulted in an increased sedimentation during glaciation during the last 2.5 Ma [*von Huene and Scholl*, 1991]. The Sunda margin however is located at low latitudes and receives almost all sediment input from the Ganges-Bahmaputra fan deposits, which arrived along the Sunda margin approximately 5 Ma [*Hamilton*, 1979]. Prior to this period, a reduced trench fill of 45% of the entire sequence is considered [*Hamilton*, 1979]. In addition, a seaward propagation of the deformation front of 2.75 km/Ma is assumed which corresponds to an Eocene onset or intensification of accretion.

[15] Analog to the trench, the solid mass equivalent of the frontal active accretionary prism in between the deformation front and the backstop (segment II in Figures 4 and 5) was gained by applying the porosity-depth relation shown in Figure 7 (prism porosity), which was also derived from the interval velocity field.

[16] From the seismic data presented here it cannot be judged unambiguously if the sediment sequence underthrusting the dynamic backstop within the subduction window is removed from the system by bypassing the static backstop or if it is underplated underneath the outer high. The mass balance calculations yield a solid mass equivalent of 1207 km^3 for the outer high off southern Sumatra (1083 km^3 off Sunda Strait and 871 km^3 off western Java). The period necessary to accrete this mass must comply with the mid- to late Eocene age of the outer high (45–37 Ma) assuming today's conditions on subduction and accretion, which are taken as a basis for the calculations. On the basis of today's conditions (e.g., convergence rate, deformation front propagation, trench input), a possible average fraction of minimum 13% (yielding an accretion period of 37 Ma) to maximum 26% (yielding 45 Ma) sediment may have been subducted along the margin to still accrete the observed mass volume in the given time range, e.g., removing 14% of the trench sequence from the system will yield an average period of accretion of 38 Ma to account for the solid fraction of the outer high (39.9 Ma off Sumatra, 38.5 Ma off Sunda Strait, 35.3 Ma off Java, corresponding to the decreasing volume of the outer high). Presuming all incoming sediment would remain in the system (0% subducted sediment), the mean period necessary to accumulate the outer high mass would be reduced by about 6.5 Ma. Mass balance calculations for the frontal accretionary prism (segment II) yield a Late Pliocene age for the material of this domain, averaging 2.6 Ma for 14% subducted trench fill.

[17] All these possible values are based on the tectonic conditions observed along the margin today. It is unlikely that the geological framework remained constant over such long periods, so the values indicated here only supply a mean average. The error bars are inversely proportional to the input error, i.e., assuming only half the convergence rate or trench fill of today's conditions will result in a time period that is doubled to what today's conditions would require. Distinct phases of the subduction history will have been characterized by varying sediment supply and convergence rate and by possible alternating phases of accretion and erosion. Assuming 30% subducted trench fill will yield an average period of 50 Ma to account for the outer high mass and a thus an initiation of subduction in the Middle to Early Eocene. Increasing this value to 50% would require a subduction period since the late Cretaceous and 80% would move this date to the Early Jurassic. Thus overall, accretion must have been the dominating process to account for the Eocene age of the outer high, which was emplaced before sedimentation filled the evolving forearc basin, where the oldest deposited strata are of Oligocene age.

6. Accretionary Mechanics

6.1. Implications From Structural Relations of Conjugate Faults

[18] The mechanics of submarine compressive accretionary prisms may be described by theoretical mechanical models, in which deforming material slides along a weak basal detachment and grows self-similar (analog to Dahlen's bulldozer wedge). The critical Coulomb wedge model [*Davis et al.*, 1983; *Dahlen*, 1990] predicts that the material within the wedge will deform under horizontal compression until a critical taper is reached and subsequently maintained. The general Coulomb criterion for shear stress τ of a cohesionless wedge at failure is of the form

$$\tau - \mu\sigma_n^*$$

where μ is the coefficient of internal friction [*Davis et al.*, 1983]. σ_n^* is the effective stress and equals $\sigma_n = p_f$ with σ_n denoting the vertical compressive stress and p_f denoting the fluid pressure. The shear stress at the detachment is of equivalent form employing the analogue basal values. A weak detachment is thus a consequence of either intrinsically weak material at the base showing a low coefficient of

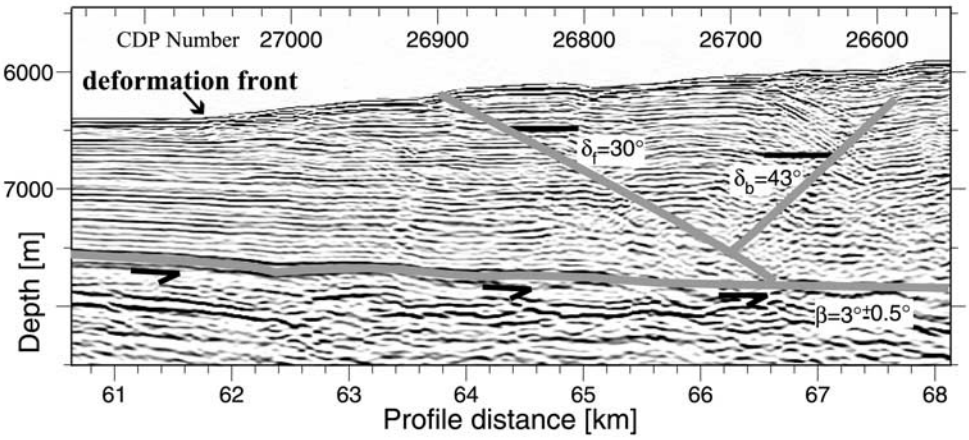

Figure 8. Detailed view of the deformation front and lower slope along the Sunda Strait transect. The structural analysis of the Sunda accretionary wedge is based on the geometry of the conjugate pair of forethrust and back thrust imaged in the depth-migrated profile. The relative dip angles of the thrusts to the décollement are gained from the relation $\delta_{\mathrm{Frel}} = \delta_f - \beta$ and $\delta_{\mathrm{Brel}} = \delta_b + \beta$.

basal friction μ_b or of a high degree of overpressuring at the base, or, as is most common, a combination of both. Analysis of structures within an accretionary prism, which is assumed to be a Coulomb wedge under horizontal compression (i.e., brittle fracture and frictional sliding occur), allows estimates on the angle ϕ and coefficient μ of internal friction and the basal stress orientation Ψ_b. Structural resolution of the Sunda Strait transect after prestack depth migration is sufficient to determine angular relations among a pair of conjugate thrust faults and the décollement (Figure 8). A prominent forethrust cuts the sedimentary sequence from the seafloor down to the décollement. Its conjugate back thrust is not as clearly imaged, but may be identified from truncated horizontal reflections. It offsets the seafloor near CDP 26600 and merges with the forethrust at CDP 26700. This pristine conjugate pair has not been rotated yet and the next pair of conjugate thrusts toward the deformation front has not fully developed and may only faintly be anticipated. Earlier error analyses [*Gutscher*, 1996] have shown that employing a pristine fault set is crucial for this method as a wrong estimate of Ψ_b (e.g., due to slight rotation) will yield a 2.7 times larger error of μ.

[19] From the dip angles of the thrusts (δ_f and δ_b in Figure 8) a basal stress orientation of $\Psi_b = 9.5°$ is derived [*Davis and von Huene*, 1987]. This direction of maximum compressive stress with the décollement follows from

$$\Psi_b = (\delta_{\mathrm{Brel}} - \delta_{\mathrm{Frel}})/2$$

The angle of internal friction ϕ may be derived from the relation

$$\phi = 90° - \delta_{\mathrm{Brel}} - \delta_{\mathrm{Frel}}$$

and is determined to be 17°. The coefficient of internal friction $\mu = \tan\phi$ then equals 0.31. Sediments of the frontal part of the accretionary wedge show only low cohesion, as the thrusts disclose neglectable bending (Figure 8) near the deformation front. For low cohesion, the direction of maximum compressive stress Ψ_b is related to the coefficients of friction of the wedge (μ) and the detachment zone (μ_b) by

$$\Psi_b = \frac{1}{2}\arcsin(\sin\phi_{\mathrm{beff}}/\sin\phi) - \frac{1}{2}\phi_{\mathrm{beff}}$$

where ϕ_{beff} is the angle of basal friction, from which the effective basal friction $\mu_{\mathrm{beff}} = \tan\phi_{\mathrm{beff}}$ may be derived after rearranging [*Kukowski et al.*, 2001]:

$$\mu_{\mathrm{beff}} = \sin(2\Psi_b)/(1/\sin\phi - \cos(2\Psi_b)) = 0.1316$$

The effective basal friction μ_{beff} accounts for variations in fluid pressure in the prism (λ) and along the detachment (λ_b):

$$\mu_{\mathrm{beff}} = \mu_b(1-\lambda_b)/(1-\lambda)$$

where λ is the ratio of fluid pressure to overburden pressure of Hubbert and Rubey [*Davis et al.*, 1983]. The ratio μ/μ_{beff} then expresses the strength ratio between the detachment zone and the sediment wedge above, as discussed, e.g., by *Davis and von Huene* [1987] and *Kukowski et al.* [2001]. As a result, the accreted sedimentary sequences along the Sunda Strait transect should be 2.3 times stronger than the detachment zone, either resulting from intrinsically weak material or from overpressuring near the base.

6.2. Effective Stress Analyses

[20] Investigations on the effective stress along the detachment will yield information on the fluid pressure ratio λ. Seismic velocities determined by focusing analyses during the prestack depth migration are converted to porosities using a standard velocity-density relationship as described above for the decompaction of the trench sediments (Figure 7). The porosity-depth relationship follows an

exponential decay corresponding to Athy's law [*Fruehn et al.*, 1997] of the form

$$\Phi = \Phi_0 \exp\{-z/c\}$$

where Φ is the porosity and Φ_0 is the porosity at the seafloor, z is depth and c = 1.65 km is the compaction length. Using the definition of the effective stress σ_n^* in terms of λ yields

$$\sigma_n^* = (1-\lambda)\rho g z$$

where g is acceleration due to gravity. By eliminating z, porosities may be expressed as a function of λ:

$$\Phi = \Phi_0 \exp\{-((1-\lambda)\rho d/(\rho_w - \rho)c)\}$$

where ρ is density, ρ_w is water density, and d is depth below seafloor [*Allen and Allen*, 1990]. Determining λ from this relationship yields slight overpressuring within the frontal prism (λ = 0.46) and only marginal higher values at the basal detachment (λ_b = 0.47). Pressure conditions throughout the prism thus remain nearly constant ($\lambda_b \approx \lambda$) and the coefficient of basal friction is only slightly larger than its effective value (μ_{beff} = 0.1316 and μ_b = 0.1346), accounting for the strength contrast of the overlying sediments to the weak décollement ($\mu_b < \mu$).

[21] The shear stress at the base, which describes the frictional sliding resistance, is given by:

$$\tau_b = (\rho - \rho_w) g d \alpha + (1-\lambda) K \rho g d (\alpha + \beta)$$

In the case of the prescribed physical properties μ, μ_b, and $\lambda_b \approx \lambda$, the dimensionless coefficient K may be derived directly from the angles of internal and basal friction ϕ and ϕ_b, respectively [*Davis et al.*, 1983]. The low values of internal and basal friction encountered at the Sunda margin correspond to a value of K = 0.8. The frictional sliding resistance τ_b is thus counteracted by two effects: the first term is due to gravity acting on the slope of the accretionary prism ("glacier term"), while the second term results from the horizontal compression ("bulldozer term") [*Davis et al.*, 1983]. For the Sunda margin, the second term is about 20% larger than the glacier term, so that compressive stresses are an important, though not a sole dominating contribution to the basal shear stress.

7. Discussion

[22] The lateral variations in material strength along the Sunda margin play a crucial role in the evolution of the structural characteristics of this subduction zone. Fluctuations in internal as well as basal friction are directly linked to surface expressions along the forearc. An increase in internal material strength from the frontal accretionary prism (segment II) to the outer high (segment III) may be inferred from the increase in seismic velocities here. The stronger material supports a narrower wedge while still undergoing stable sliding at its base. This results in a decrease in surface slope landward of the out-of-sequence thrust. This effect is also witnessed at other accretionary subduction zones (e.g., Barbados accretionary wedge [*Bangs et al.*, 1990] or Alaska margin [*Ryan and Scholl*, 1989; *Fruehn et al.*, 1999]). Variations in the surface slope may alternatively evolve from fluctuations in basal friction, possibly resulting from a change in stratigraphy of the décollement material, or for areas where Coulomb behavior is no longer valid. Reduced basal resistance is expected beneath the outer high, as it occurs below the brittle-plastic transition below 12–16 km depth [*Davis et al.*, 1983]. It is here that the surface slope is shallowest (Figure 6) as a response to the plastic sliding along the detachment at greater depth. The surface slopes of individual thrust slices or accretionary ridges may be significantly steeper, though, as they are governed by the friction along the adjacent thrusts cutting through the stronger upper section of the accretionary prism. As the material composing the individual ridges is dehydrated and becomes stronger, thus showing a positive gradient in the coefficient of internal friction, the ridges may become supercritical. This is observed in the bathymetry, e.g., off southern Sumatra, where slumps and slides manifest an unstable regime.

[23] Overpressuring along the Sunda margin is insignificant, as most pore fluids have already been expelled near the deformation front where the numerous fractures act as conduits [*Faber et al.*, 2001; *Kopp*, 2002]. Dewatering is highly effective across stratigraphically controlled boundaries in the presence of fluid migration paths [*von Huene and Klaeschen*, 1999], prohibiting high pore pressures in the detachment zone. Thus dewatering likely contributes to the laterally increasing material strength, which leads to a segmentation of the frontal part of the margin and is also linked to the loss in brightness of the reflections in segment III. The composition, grain size, or conditions during sedimentation may also influence the low overpressuring. Comparably low values of basal friction and overpressuring have also been reported from the Makran accretionary wedge bordering the northern Indian Ocean [*Fruehn et al.*, 1997; *Kukowski et al.*, 2001], while high pore fluid pressures have been inferred for most other accretionary complexes (e.g., Alaska, Barbados, Nankai, Cascadia) [*Davis et al.*, 1983; *Lallemand et al.*, 1994]. Another similarity between Makran and Sunda is the intrinsic strength contrast between the décollement and the overlying sediments [*Kukowski et al.*, 2001].

[24] The mechanical properties of the wedge are essential for the material transfer. On the basis of the mass balance calculations, a possible scenario to account for the Eocene age of the outer high would imply that on average less than 30% of the sediment input is subducted and passes the static backstop. Frontal accretion is the dominant mode of transfer along the Sunda margin, and only a low percentage of sediment is underplated or subducted, similar to the situation along the Cascadia margin [*Davis and Hyndman*, 1989]. However, when new basal material transported into the subduction zone has properties such that $(1-\lambda_b)\mu_b > (1-\lambda)\mu$, it cannot form a décollement and a new décollement

must form higher in the wedge, leading to tectonic erosion. For an earlier phase of higher basal friction, a prism may partially be supercritical. Local variations of the surface slope along the Nankai accretionary wedge have been attributed to fluctuations in basal friction [*Moore et al.*, 1990]. Along the central Sunda margin, the dip of the décollement remains constant at ≈3°, whereas the surface slope decreases from ≈5.5° off Sumatra to 3° off Java. This slight decrease in surface slope may be caused by minor changes in material and basal properties. On a smaller scale, fluctuations in basal friction may also be linked to the local retreat of the deformation front off southern Sumatra, as recognized in the bathymetry image displayed in Figure 2. However, a detailed evaluation lies beyond the scope of the data.

[25] The structural effects resulting from a Sunda-type backstop geometry have been reproduced in analogue and numerical modeling [e.g., *Malavieille et al.*, 1993; *Byrne et al.*, 1993; *Buck and Sokoutis*, 1994; *Kukowski et al.*, 1994; *Wang and Davis*, 1996]. In the experiments, an outer high always developed in the presence of a strong trenchward dipping backstop, accompanied by the evolution of a depression between the morphological high and the arc, which becomes a forearc basin upon sedimentation [*Larroque et al.*, 1995]. Subcrustal erosion may enhance forearc basin evolution. It has been shown that the morphological effects are most pronounced for a seaward dipping backstop (type I geometry of Byrne). The growth of an outer high is diminished for a landward dipping backstop (type II geometry of Byrne) or intermediate geometry (i.e., toe of static backstop occurs at shallower depth within forearc), as have been mapped along the Cascadia and Peru margins, respectively [*Davis and Hyndman*, 1989; *von Huene et al.*, 1988]. Even though several types of backstops may exist simultaneously within a single margin, similar structural features resulting from backstop mechanics are predicted by modeling, even in the presence of a complex or multiple backstop [*Byrne et al.*, 1993] and are observed in nature along the Sunda margin. The existence of multiple backstops has also been proposed for the accretionary Barbados wedge [*Byrne et al.*, 1993] and is also inferred for the erosional Peru margin (A. Krabbenhoeft, personal communication, 2000) as well.

8. Conclusions

[26] Employing different data acquisition methods for the first time enables the exact mapping of the backstop system geometry along the Sunda subduction zone. An additional important aspect of this study is the observation that the structural elements characteristic for this subduction zone are present in regimes of frontal convergence in the east as well as in regimes of oblique convergence to the northwest. Oblique convergence was addressed by analogue modeling [*Calassou et al.*, 1993], which found that the main structural features perpendicular to the backstop would always develop, even for highly oblique convergence like off northern Sumatra. *Fitch* [1972] discussed the evolution of strike-slip faults along oblique convergence zones to compensate the lateral component of motion. Strike-slip faulting was reproduced in analogue experiments, where flower structures would develop near the static backstop [*Calassou et al.*, 1993]. Along the Sunda margin, the Mentawai fault zone has been proposed to take up the majority of displacement along strike [*Diament et al.*, 1992], though a stretching of the forearc sliver has also been inferred from geodetic data and slip vectors [*Fitch*, 1972; *Moore et al.*, 1980; *McCaffrey*, 1992; *McCaffrey et al.*, 2000].

[27] The Sunda plate boundary along its northern and central part represents a classic accretionary margin and in view of the low percentage of subducted trench material poses an end-member for this class of subduction zones. The geological framework of a subduction zone, namely the material input, the oceanic plate roughness, and the convergence rate, control whether accretion or erosion will dominate. The formation of the décollement is fundamentally linked to the mechanical properties of the progressing frontal prism and is essential for the size of the subduction window. The stress reduction observed along the Sunda décollement results from the intrinsically weak material observed here. Excess fluid pressures, which have been found to play a dominant role in a number of subduction zones, are inhibited along the Sunda margin by the intense degree of faulting and fracturing which is initiated in the trench and intensified along the frontal active accretionary prism. The evolution of morphological features, foremost of the outer high and forearc basin, however, are ruled by backstop dynamics above the static backstop. As accretion has remained stable along this margin, the outer high evolved as a consolidated and tectonically quiescent dynamic backstop, which controls recent accretionary processes.

[28] **Acknowledgments.** We are indebted to the BGR, Hannover, Germany, for providing the MCS and Bathymetry data collected during cruises SO137 and SO139 of R/V Sonne. Many thanks to the participants of the GINCO cruises for their help with data acquisition and preprocessing. Capt. Papenhagen and his crew ably assisted us at sea. We kindly acknowledge the help of W. Weinrebe with the processing of the Hydrosweep data and thank D. Klaeschen for support during prestack depth migration. We thank J. Lohrmann for discussions concerning wedge mechanics. Discussions with C. Kopp and A. Kopf helped clarify aspects on mass balancing. We thank E. R. Flueh for comments on the manuscript. Careful reviews by G. Moore, Associate Editor D. Cowan and Editor B. Wernicke helped tighten the manuscript considerably.

References

Allen, P. A., and J. R. Allen, *Basin Analysis: Principles and Applications*, Blackwell Sci., 451 pp., Malden, Mass., 1990.

Bangs, N. L. B., G. K. Westbrook, J. W. Ladd, and P. Buhl, Seismic velocities from the Barbados Ridge Complex: Indicators of high pore fluid pressures in an accretionary complex, *J. Geophys. Res.*, *95*, 8767–8782, 1990.

Beaudry, D., and G. Moore, Seismic-stratigraphic framework of the forearc basin off central Sumatra, Sunda Arc, *Earth Planet. Sci. Lett.*, *54*, 17–28, 1981.

Beaudry, D., and G. Moore, Seismic stratigraphy and Cenozoic evolution of west Sumatra forearc basin, *AAPG Bull.*, *69*, 742–759, 1985.

Bray, C. J., and D. E. Karig, Porosity of sediments in accretionary prisms and some implications for dewatering processes, *J. Geophys. Res.*, *90*(B1), 768–778, 1985.

Buck, W. R., and D. Sokoutis, Analogoue model of gravitational collapse and surface extension during continental convergence, *Nature*, *369*, 737–740, 1994.

Byrne, D. E., W.-H. Wang, and D. M. Davis, Mechanical role of backstops in the growth of forearcs, *Tectonics*, *12*, 123–144, 1993.

Calassou, S., C. Larroque, and J. Malavieille, Transfer zones of deformation in thrust wedges: An experimental study, *Tectonophysics*, *221*, 325–344, 1993.

Caress, D. W., and D. N. Chayes, Improved processing of Hydrosweep DS multibeam data on the R/V *Maurice Ewing*, *Mar. Geophys. Res.*, *18*, 631–650, 1996.

Dahlen, F. A., Critical taper model of fold-and-thrust belts and accretionary wedges, *Annu. Rev. Earth Planet. Sci.*, *18*, 55–99, 1990.

Davis, D. M., Accretionary mechanics with properties that vary in space and time, in *Subduction: Top to Bottom*, *Geophys. Monogr. Ser.*, vol. 96, pp. 39–48, edited by G. E. Bebout et al., AGU, Washington, D. C., 1996.

Davis, E. E., and R. Hyndman, Accretion and recent deformation of sediments along the northern Cascadia subduction zone, *Geol. Soc. Am. Bull.*, *101*, 1465–1480, 1989.

Davis, D. M., and R. von Huene, Inferences on sediment strength and fault friction from structures at the Aleutian Trench, *Geology*, *15*, 517–522, 1987.

Davis, D. M., J. Suppe, and F. A. Dahlen, Mechanics of fold-and-thrust belts and accretionary wedges, *J. Geophys. Res.*, *88*, 1153–1172, 1983.

Diament, M., C. Deplus, H. Harjono, M. Larue, O. Lassal, J. Dubois, and V. Renard, Extension in the Sunda Strait (Indonesia): A review of the Krakatau programme, *Oceanol. Acta, Spec.* Vol., 10, 31–42, 1990.

Diament, M., H. Harjono, K. Karta, C. Deplus, D. Dahrin, M. T. Zan Jr., M. Gerard, O. Lassal, A. Martin, and J. Malod, Mentawai fault zone off Sumatra: A new key to the geodynamics of western Indonesia, *Geology*, *20*, 259–262, 1992.

Faber, E., J. Poggenburg, and W. Stahl, Methane in water and sediments, in *Summary and Synthesis of RV Sonne Cruises SO137-139 and Final Report Cruise SO139*, edited by H. Beiersdorf, *BGR Rep. 10815/01*, vol. *IV*, pp. 1–25, 2001.

Fitch, T. J., Plate convergence, transcurrent faults and internal deformation adjacent to Southeast Asia and the western Pacific, *J. Geophys. Res.*, *77*, 4432–4460, 1972.

Flueh, E. R., and J. Bialas, A digital, high data capacity ocean bottom recorder for seismic investigations, *Int. Underwater Syst. Design*, *18*(3), 18–20, 1996.

Flueh, E. R., and Shipboard Science Party, GINCO2 (*Sonne* Cruise SO-138): Geo-scientific investigations along the active convergence zone between the eastern Eurasian and Indo-Australian Plates off Indonesia, cruise report, Geomar, Kiel, Germany, 1999.

Font, Y., C.-S. Liu, P. Schnuerle, and S. Lallemand, Constraints on backstop geometry of the southwest Ryukyu subduction based on reflection seismic data, *Tectonophysics*, *333*, 135–158, 2001.

Fruehn, J., R. S. White, and T. A. Minshull, Internal deformation and compaction of the Makran accretionary wedge, *Terra Nova*, *9*, 101–104, 1997.

Fruehn, J., R. von Huene, and M. A. Fisher, Accretion in the wake of terrane collision: The Neogene accretionary wedge off Kenai peninsula, *Alaska, Tectonics*, *18*, 263–277, 1999.

Grant, J. A., and R. Schreiber, Modern swath sounding and subbottom profiling technology for research applications: The Atlas Hydrosweep and Parasound systems, *Mar. Geophys. Res.*, *12*, 9–19, 1990.

Gutscher, M.-A., Growth, erosion and material transfer in accretionary wedges: A quantitative analysis based on analog modeling and the implications for the evolution of convergent margins, Ph.D. thesis, Univ. Kiel, Kiel, Germany, 1996.

Hamilton, E. L., Sound velocity-density relations in sea-floor sediments and rocks, *J. Acoust. Soc. Am.*, *63*, 366–377, 1978.

Hamilton, W., Tectonics of the Indonesian region, *U.S. Geol. Surv. Prof. Pap.*, *1078*, 1979.

Hamilton, W., Plate tectonics and island arcs, *Geol. Soc. Am. Bull.*, *100*, 1503–1527, 1988.

Huchon, P., and X. Le Pichon, Sunda Strait and central Sumatra fault, *Geology*, *12*, 668–672, 1984.

Izart, A., B. Mustafa Kemal, and J. A. Malod, Seismic stratigraphy and subsidence evolution of the northwest Sumatra fore-arc basin, *Mar. Geol.*, *122*, 109–124, 1994.

Kieckhefer, R. M., G. F. Moore, and F. J. Emmel, Crustal structure of the Sunda forearc region west of central Sumatra from gravity data, *J. Geophys. Res.*, *86*, 7003–7012, 1981.

Kopf, A., D. Klaeschen, and J. Mascle, Extreme efficiency of mud volcanism in dewatering accretionary prisms, *Earth Planet. Sci. Lett.*, *189*, 295–313, 2001.

Kopp, H., BSR occurrence along the Sunda margin: Evidence from seismic data, *Earth Planet. Sci. Lett.*, *197*, 225–235, 2002.

Kopp, H., E. R. Flueh, D. Klaeschen, J. Bialas, and C. Reichert, Crustal structure of the central Sunda margin at the onset of oblique subduction, *Geophys. J. Int.*, *147*, 449–474, 2001.

Kopp, H., D. Klaeschen, E. R. Flueh, J. Bialas, and C. Reichert, Crustal structure of the Java margin from seismic wide-angle and multichannel reflection data, *J. Geophys. Res.*, *107*(B2), 2034, doi:10.1029/2000JB000095, 2002.

Kukowski, N., R. von Huene, J. Malavieille, and S. E. Lallemand, Sediment accretion against a buttress beneath the Peruvian continental margin as simulated with sandbox modeling, *Geol. Rundsch.*, *83*, 822–831, 1994.

Kukowski, N., T. Schillhorn, K. Huhn, U. von Rad, S. Husen, and E. R. Flueh, Morphotectonics and mechanics of the central Makran accretionary wedge off Pakistan, *Mar. Geol.*, *173*, 1–19, 2001.

Lallemand, S. E., P. Schnuerle, and J. Malavieille, Coulomb theory applied to accretionary and nonaccretionary wedges: Possible causes for tectonic erosion and/or frontal accretion, *J. Geophys. Res.*, *99*, 12,033–12,055, 1994.

Larroque, C., S. Calassou, J. Malavieille, and F. Chanier, Experimental modelling of forearc basin development during accretionary wedge growth, *Basin Res.*, *7*, 255–268, 1995.

Lelgemann, H., M.-A. Gutscher, J. Bialas, E. R. Flueh, W. Weinrebe, and C. Reichert, Transtensional basins in the western Sunda Strait, *Geophys. Res. Lett.*, *27*, 3545–3548, 2000.

Lohrmann, J., N. Kukowski, J. Adam, and O. Oncken, The impact of analogue material properties on the geometry, kinematics, and dynamics of convergent sand wedges, *J. Struct. Geol.*, *27*(21), 3545–3548, 2002.

Mackay, S., and R. Abma, Depth focusing analysis using wavefront-curvature criterion, *Geophysics*, *58*, 1148–1156, 1993.

Malavieille, J., Modelization exprimentale des chevauchements imbriqus: Application aux chaines de mountagnes, *Bull. Soc. Geol. Fr.*, *7*, 129–138, 1984.

Malavieille, J., C. Larroque, and S. Calassou, Modelization experimentale des relations tectonique-sedimentation entre bassin avant-arc et prisme d'accretion, *C. R. Acad. Sci., Ser. II*, *316*, 1131–1137, 1993.

Malod, J. A., and B. M. Kemal, The Sumatra margin: Oblique subduction and lateral displacement of the accretionary prism, in *Tectonic Evolution of Southeast Asia*, edited by R. Hall and D. Blundell, *Geol. Soc. Spec. Publ.*, *106*, 19–28, 1996.

Malod, J. A., K. Karta, M. O. Beslier, and M. T. Zen Jr., From normal to oblique subduction: Tectonic relationships between Java and Sumatra, *J. SE Asian Earth Sci.*, *12*, 85–93, 1995.

McCaffrey, R., Oblique plate convergence, slip vectors, and forearc deformation, *J. Geophys. Res.*, *97*, 8905–8915, 1992.

McCaffrey, R., Slip partitioning at convergent plate boundaries of SE Asia, in *Tectonic Evolution of Southeast Asia*, edited by R. Hall and D. Blundell, *Geol. Soc. Spec. Publ.*, *106*, 3–18, 1996.

McCaffrey, R., P. C. Zwick, Y. Bock, L. Prawirodirdjo, J. F. Genrich, C. W. Stevens, S. S. O. Puntodewo, and C. Subarya, Strain partitioning during oblique plate convergence in northern Sumatra: Geodetic and seismologic constraints and numerical modeling, *J. Geophys. Res.*, *105*, 28,363–28,376, 2000.

Moore, G. F., and D. E. Karig, Structural geology of Nias Island, Indonesia: Implications for subduction zone tectonics, *Am. J. Sci.*, *280*, 193–223, 1980.

Moore, G. F., J. R. Curray, D. G. Moore, and D. E. Karig, Variations in geologic structure along the Sunda fore arc, northeastern Indian Ocean, in *The Tectonic and Geologic Evolution of Southeast Asian Seas and Islands*, *Geophys. Monogr. Ser.*, vol. 23, edited by D. Hayes, pp. 145–160, AGU, Washington, D. C., 1980.

Moore, G. F., J. R. Curray, and F. J. Emmel, Sedimentation in the Sunda trench and forearc region, in *Trench-Forearc Geology*, edited by J. K. Leggett, *Geol. Soc. Spec. Publ.*, *10*, 245–258, 1982.

Moore, G. F., T. H. Shipley, P. L. Stoffa, D. E. Karig, A. Taira, S. Kuramoto, H. Tokuyama, and K. Suyehiro, Structure of the Nankai Trough Accretionary Zone from multichannel seismic reflection data, *J. Geophys. Res.*, *95*, 8753–8765, 1990.

Prawirodirdjo, L., Y. Bock, J. F. Genrich, S. S. O. Puntodewo, J. Rais, C. Subarya, and S. Sutisna, One century of tectonic deformation along the Sumatran fault from triangulation and Global Positioning System surveys, *J. Geophys. Res.*, *105*, 28,343–28,361, 2000.

Pubellier, M., C. Rangin, J.-P. Cadet, I. Tjashuri, J. Butterlin, and C. Mueller, L'ile de Nias, un edifice polyphase sur la bordure interne de la fosse de la Sonde (Archipel de Mentawai, Indonesie), *C. R. Acad. Sci., Ser. II*, *8*, 1019–1026, 1992.

Ranero, C. R., and R. von Huene, Subduction erosion along the Middle America convergent margin, *Nature*, *404*, 748–752, 2000.

Reichert, C., and Shipboard Science Party, GINCO1 (*Sonne* Cruise SO-137): Geo-scientific investigations along the active convergence zone between the eastern Eurasian and Indo-Australian Plates off Indonesia, cruise report, BGR, Hannover, Germany, 1999.

Ryan, H. F., and D. W. Scholl, The evolution of forearc structures along an oblique convergent margin, central Aleutian arc, *Tectonics*, *8*, 497–516, 1989.

Samuel, M. A., and N. A. Harbury, The Mentawai fault zone and deformation of the Sumatran forearc in the Nias area, in *Tectonic Evolution of Southeast Asia*, edited by R. Hall and D. Blundell, *Geol. Soc. Spec. Publ.*, *106*, 337–351, 1996.

Schlüter, H. U., C. Gaedicke, H. A. Roeser, B. Schreckenberger, H. Meyer, C. Reichert, Y. Djajadihardja, and A. Prexl, Tectonic features of the southern Sumatra-western Java forearc of Indonesia, *Tectonics*, *21*(5), 1047, doi:10.1029/2001TC901048, 2002.

Sieh, K., and D. Natawidjaja, Neotectonics of the Sumatran fault, Indonesia, *J. Geophys. Res.*, *105*, 28,295–28,326, 2000.

Tregoning, P., F. K. Brunner, Y. Bock, S. S. O. Puntodewo, R. McCaffrey, J. F. Genrich, E. Calais, J. Rais, and C. Subarya, First geodetic measurement of

convergence across the Java Trench, *Geophys. Res. Lett.*, *21*, 2135–2138, 1994.

von Huene, R., and D. Klaeschen, Opposing gradients of permanent strain in the aseismic zone and elastic strain across the seismogenic zone of the Kodiak shelf and slope, Alaska, *Tectonics*, *18*, 248–262, 1999.

von Huene, R., and D. W. Scholl, Observations at convergent margins concerning sediment subduction, subduction erosion and the growth of continental crust, *Rev. Geophys.*, *29*, 279–316, 1991.

von Huene, R., E. Suess, and Leg 112 Shipboard Scientists, Ocean drilling program Leg 112, Peru continental margin: Part I, tectonic history, *Geology*, *16*, 934–938, 1988.

von Huene, R., D. Klaeschen, M. Gutscher, and J. Fruehn, Mass and fluid flux during accretion at the Alaskan margin, *Geol. Soc. Am. Bull.*, *110*, 468–482, 1998.

Wang, W.-H., and D. M. Davis, Sandbox model simulation of forearc evolution and noncritical wedges, *J. Geophys. Res.*, *101*, 11,329–11,339, 1996.

Wessel, P., and W. H. F. Smith, Free software helps map and display data, *Eos Trans. AGU*, *72*, 441, 445–446, 1991.

H. Kopp, GEOMAR Research Center for Marine Geosciences, Wischhofstr. 1-3, D-24148 Kiel, Germany. (hkopp@geomar.de)

N. Kukowski, GFZ GeoForschungszentrumPotsdam, Telegrafenberg, D-14473 Potsdam, Germany. (nina@gfz-potsdam.de)